JACS
JOURNAL OF THE AMERICAN CHEMICAL SOCIETY
pubs.acs.org/JACS
Article

Self-Assembled Homopolymeric Spherulites from Small Molecules in Solution

Qiantao Song,[○] Yi Li,[○] Zhicheng Jin, Hai Liu, Matthew N. Creyer, Wonjun Yim, Yanping Huang, Xiaobing Hu, Tengyu He, Yajuan Li, Shana O. Kelley, Lingyan Shi, Jiajing Zhou,* and Jesse V. Jokerst*

Cite This: J. Am. Chem. Soc. 2023, 145, 25664−25672

Read Online

ACCESS | Metrics & More | Article Recommendations | Supporting Information

ABSTRACT: Polymeric spherulites are typically formed by melt crystallization: spherulitic growth in solution is rare and requires complex polymers and dilute solutions. Here, we report the mild and unique formation of luminescent spherulites at room temperature via the simple molecule benzene-1,4-dithiol (BDT). Specifically, BDT polymerized into oligomers (PBDT) via disulfide bonds and assembled into uniform supramolecular nanoparticles in aqueous buffer; these nanoparticles were then dissolved back into PBDT in a good solvent (i.e., dimethylformamide) and underwent chain elongation to form spherulites (rPBDT) in 10 min. The spherulite geometry was modulated by changing the PBDT concentration and reaction time. Due to the step-growth polymerization and reorganization of PBDT, these spherulites not only exhibited robust structure but also showed broad clusterization-triggered emission. The biocompatibility and efficient cellular uptake of the spherulites further underscore their value as traceable drug carriers. This system provides a new pathway for designing versatile superstructures with value for hierarchical assembly of small molecules into a complicated biological system.

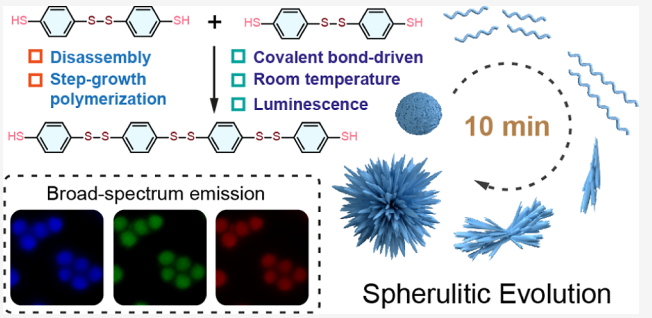

INTRODUCTION

Self-assembly is ubiquitous in nature.[1−6] Natural molecules such as amino acids, peptides, proteins, and DNA can form cooperative self-assemblies that execute vital biological functions.[7−11] Such self-assembly can be considered a versatile bottom-up synthesis method and has led to a myriad of functional hierarchical structures in life science and materials engineering.[12−16] Spherulites are one type of self-assembled systems and polycrystalline structures in which acicular crystals radiate from a common center and grow nearly synchronously, leading to a spherical structure. Indeed, spherulites can be obtained from a wide range of materials (e.g., metals, minerals, organic molecules, proteins, and synthetic polymers) and have garnered extensive attention in drug delivery, tissue engineering, and sensing.[17−23] Moreover, manipulating the formation of spherulites is an important topic in biological systems. For example, the formation of spherulites by amyloid fibers has been linked to neurodegenerative pathologies (e.g., Alzheimer's diseases).[24,25] Controlling spherulite morphology and exploring the mechanism of spherulite growth are vital steps in enhancing material performance and achieving effective disease treatment.[26−28]

The most common method for preparing organic spherulites is cooling crystallization,[29−31] which involves heating a polymer solution to make it supersaturated and then cooling it rapidly to induce crystallization or directly cooling the polymer melt to form crystals. The nucleation and growth of spherulites are affected by temperature, concentration, and solvent qualities; therefore, precise control of the annealing process and solution supersaturation is critical in preparing spherulites.[32−38] For instance, neat poly(1, 6-hexamethylene adipate) spherulites transformed from negative-type spherulites (radial refractive index > tangential refractive index) at low crystallization temperatures to positive-type spherulites (tangential refractive index > radial refractive index) at high crystallization temperatures.[39] Porous spherulites were formed with isothermal crystallization of poly(L-lactide) in diethyl phthalate and glycerol tri-*n*-propionate but not in less viscous solvents like dimethyl sulfoxide (DMSO) or dimethylformamide (DMF).[40] While there are numerous examples of spherulite formation from supersaturated polymer solutions and polymer melts,[41,42] spherulite formation in dilute solutions remains a rare phenomenon. Recently, Winnik and co-workers reported the first example of spherulite formation via the self-assembly of a block copolymer in a dilute solution. They then investigated the

Received: August 2, 2023
Revised: October 15, 2023
Accepted: October 18, 2023
Published: November 3, 2023

Downloaded via UNIV OF CALIFORNIA SAN DIEGO on May 10, 2024 at 17:39:45 (UTC).
See https://pubs.acs.org/sharingguidelines for options on how to legitimately share published articles.

© 2023 American Chemical Society

https://doi.org/10.1021/jacs.3c08356
J. Am. Chem. Soc. 2023, 145, 25664−25672

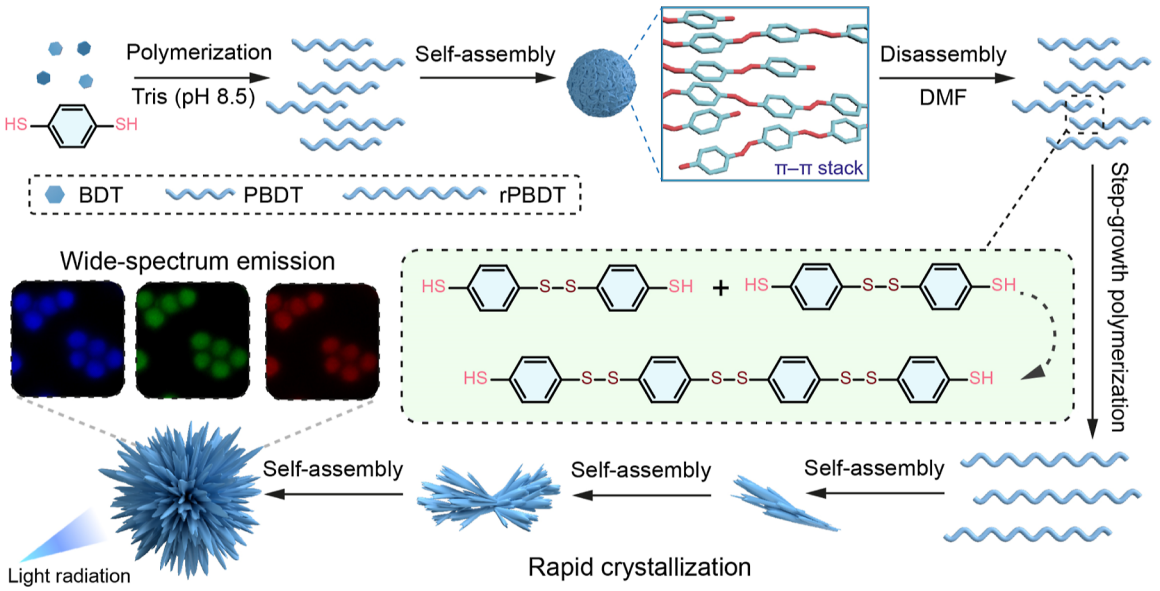

Figure 1. Process of forming rPBDT spherulites from small BDT molecules. BDT molecules form PBDT chains through disulfide bonds under alkaline conditions and then self-assemble into PBDT nanoparticles. PBDT nanoparticles disassemble into PBDT chains in DMF. The formation of disulfide bonds leads to the growth of PBDT chains into rPBDT chains, which gradually assemble to form spherulites.

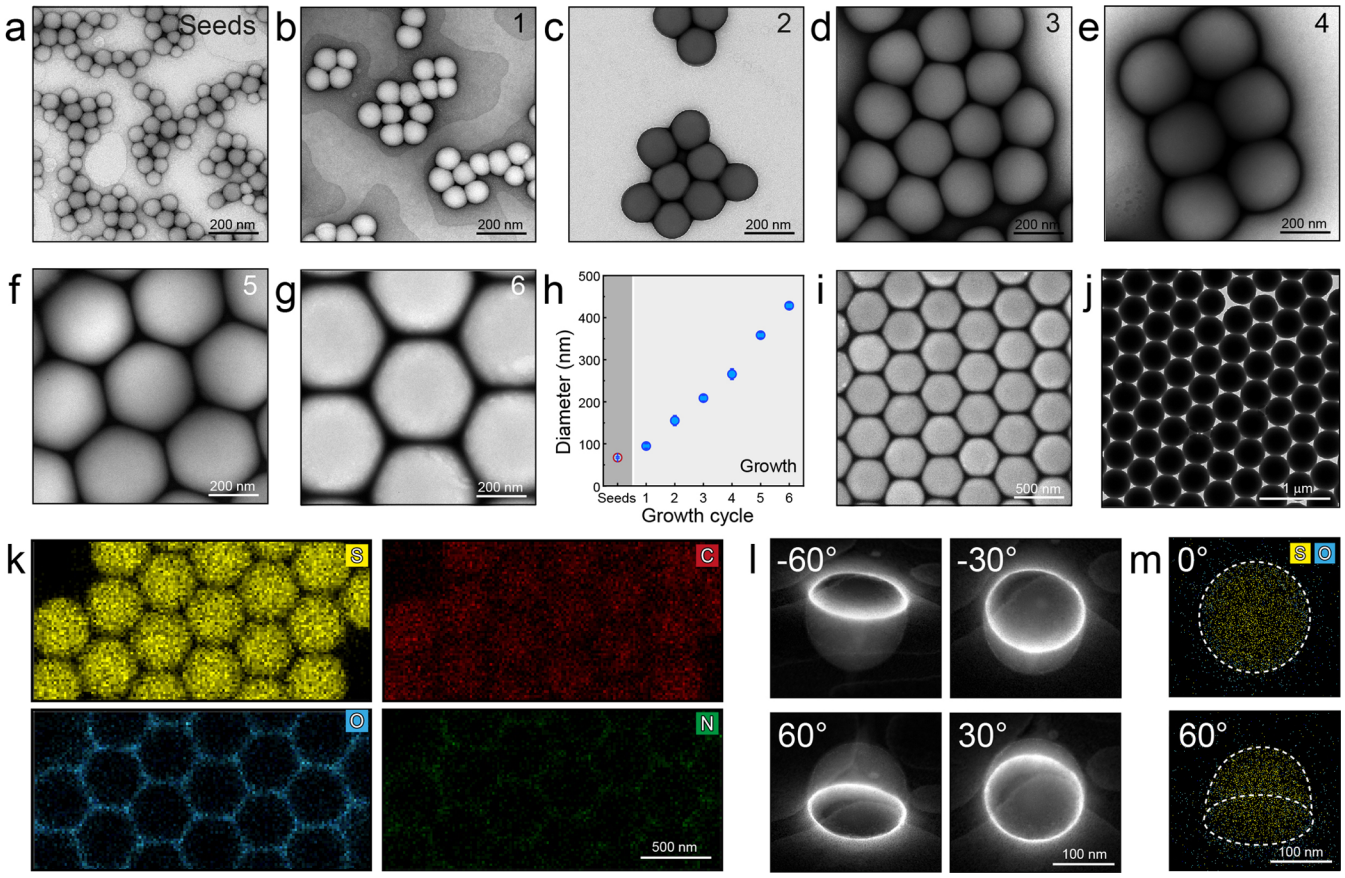

Figure 2. Synthesis of PBDT nanoparticles. (a) TEM image of PBDT nanoparticles. (b–g) TEM images of PBDT nanoparticles of different sizes prepared by seed-mediated growth. The number denoted in the upper right corner indicates the growth cycle. (h) DLS results of PBDT nanoparticles prepared by repeating seed-mediated growth . (i) SEM image of PBDT nanoparticles (450 nm) in a large population. (j) TEM image of PBDT nanoparticles (450 nm) in a large population. (k) Elemental mappings of PBDT nanoparticles. (l) TEM images of PBDT nanoparticles at different angles. (m) EDX elemental mappings of PBDT nanoparticles at different angles.

https://doi.org/10.1021/jacs.3c08356
J. Am. Chem. Soc. 2023, 145, 25664–25672

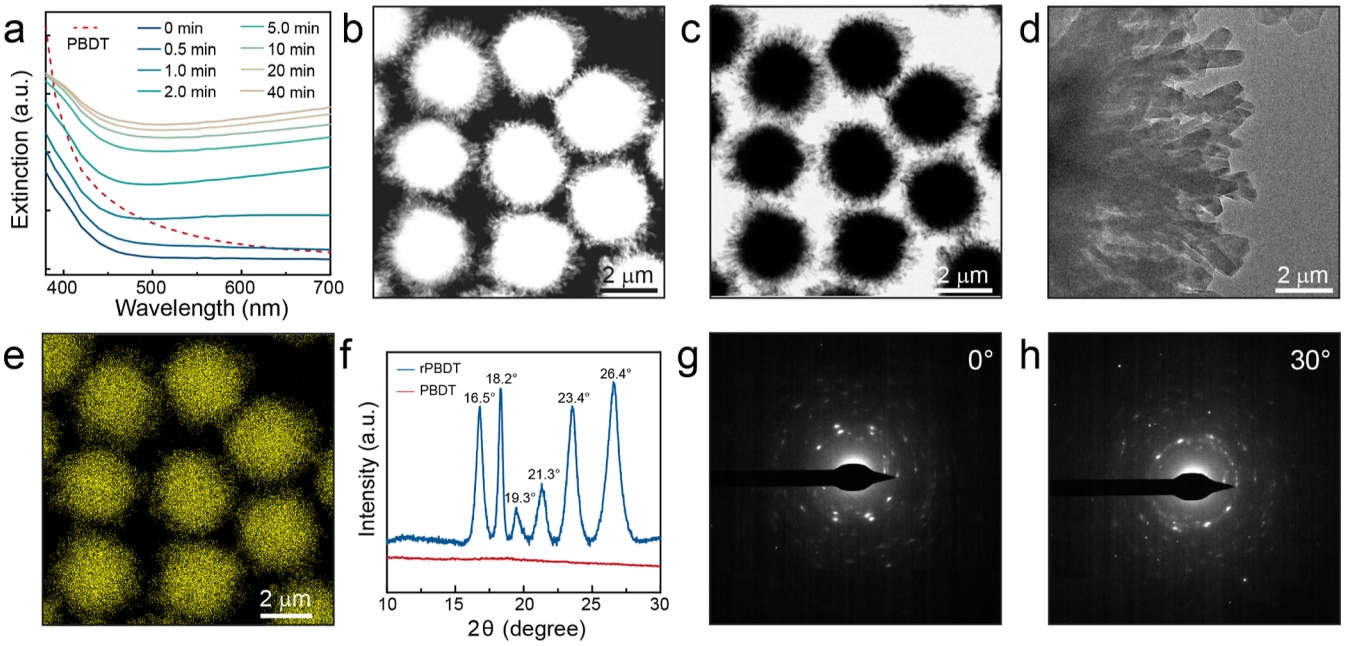

Figure 3. Synthesis of rPBDT spherulites and crystal structure characterization. (a) Time-dependent UV−vis spectra of rPBDT spherulites during the spherulitic growth. (b) HAADF image of rPBDT spherulites. (c) TEM image of rPBDT spherulites. (d) TEM image of spikes on the surface of rPBDT spherulites. (e) EDX elemental mapping of S elements in rPBDT spherulites. (f) XRD patterns of PBDT nanoparticles and rPBDT spherulites. (g,h) Cryo-SAED patterns of rPBDT spherulite at different angles.

assembly mechanism. Of note, this system still required the presynthesized nuclei and delicate control of annealing and aging.[43,44]

Understanding the morphological changes, structural evolution, and crystallization mechanisms involved in spherulite formation is a challenge due to the demanding conditions required for their growth.[45,46] We recently found that benzene-1,4-dithiol (BDT) can self-assemble into uniform supramolecular nanoparticles (PBDT) via $\pi-\pi$ stacking with disassembly in organic solvents, e.g., DMF.[47] Intriguingly, PBDT nanoparticles rapidly dissolved in DMF and then formed spherulites at room temperature within 1 min. This process did not necessitate intricate temperature control or presynthesized complex polymers. This finding motivated us to further employ this system for spherulite design. Moreover, to the best of our knowledge, the synthesis of homopolymeric spherulites from small molecules in solution remains quite rare.

Here, we report the first example of spherulite formation by the self-assembly of small molecules at room temperature (Figure 1). Specifically, BDT can self-polymerize through disulfide bonds to form polymerized uniform PBDT nanoparticles with tunable size in aqueous environment. These PBDT nanoparticles rapidly dissolve in DMF (i.e., generating dispersive PBDT molecules) and then experience step-growth polymerization via disulfide bonds while assembling into spherulites (rPBDT) within 10 min. The dynamic growth of the rPBDT spherulites indicated the unique evolution of this insoluble spherulite: the disulfide-mediated elongation of the chains from PBDT nanoparticles gives the rPBDT spherulites a higher molecular weight that then precipitates into a crystal spherulite. The rPBDT spherulites have broad luminescence performance probably due to the clusterization-triggered emission of PBDT molecules with different molecular weights. They exhibited obvious fluorescence in various media including at extreme pH conditions (pH 1 or 13). We further validated rPBDT spherulites as a biocompatible and traceable particle system. Our findings not only provide a mild fabrication strategy for uniform functional spherulites but also highlight the role of the covalent bond in spherulitic growth which has been largely overlooked.

RESULTS AND DISCUSSION

Homopolymeric PBDT nanoparticles were first synthesized. In bicine buffer (10 mM, pH 8.5), BDT molecules formed PBDT molecules via disulfide bonds, and the increased hydrophobicity led to the self-assembly of PBDT molecules into uniform nanoparticles. Transmission electron microscopy (TEM) result showed that the resulting nanoparticles were ∼70 nm in diameter (Figure S1) and had a smooth spherical morphology (Figure 2a). Interestingly, the nanoparticle size was tunable via seed-mediated growth,[48−50] and these PBDT nanoparticles can be modulated from 90 to 450 nm by repeating this protocol (Figure 2b−h). The PBDT nanoparticles prepared by seed-mediated growth maintained a smooth spherical morphology and uniform size (Figure 2i,j). It is notable that the size distribution of the products was affected by the quantity of seeds added in the growing step (Figure S2). If a low concentration of seeds (0.1 mL) was used (i.e., high ratio of BDT precursor to seed), then the nucleation and growth of free PBDT nanoparticles would occur, leading to the poor size distribution of the products. Energy-dispersive X-ray spectroscopy (EDX) results revealed that PBDT nanoparticles were mainly composed of S and C elements (Figure 2k) confirming that only BDT was involved in the formation of PBDT nanoparticles. This homogeneous system significantly streamlines this BDT workflow versus our previous system where nanoparticles comprised PBDT and tannic acid.[51] The PBDT nanoparticles were a soft material that deformed during drying (Figures 2l,m, and Figure S3).

Next, the assembly process of PBDT nanoparticles into rPBDT spherulite was investigated. In a typical process, the as-

https://doi.org/10.1021/jacs.3c08356
J. Am. Chem. Soc. 2023, 145, 25664−25672

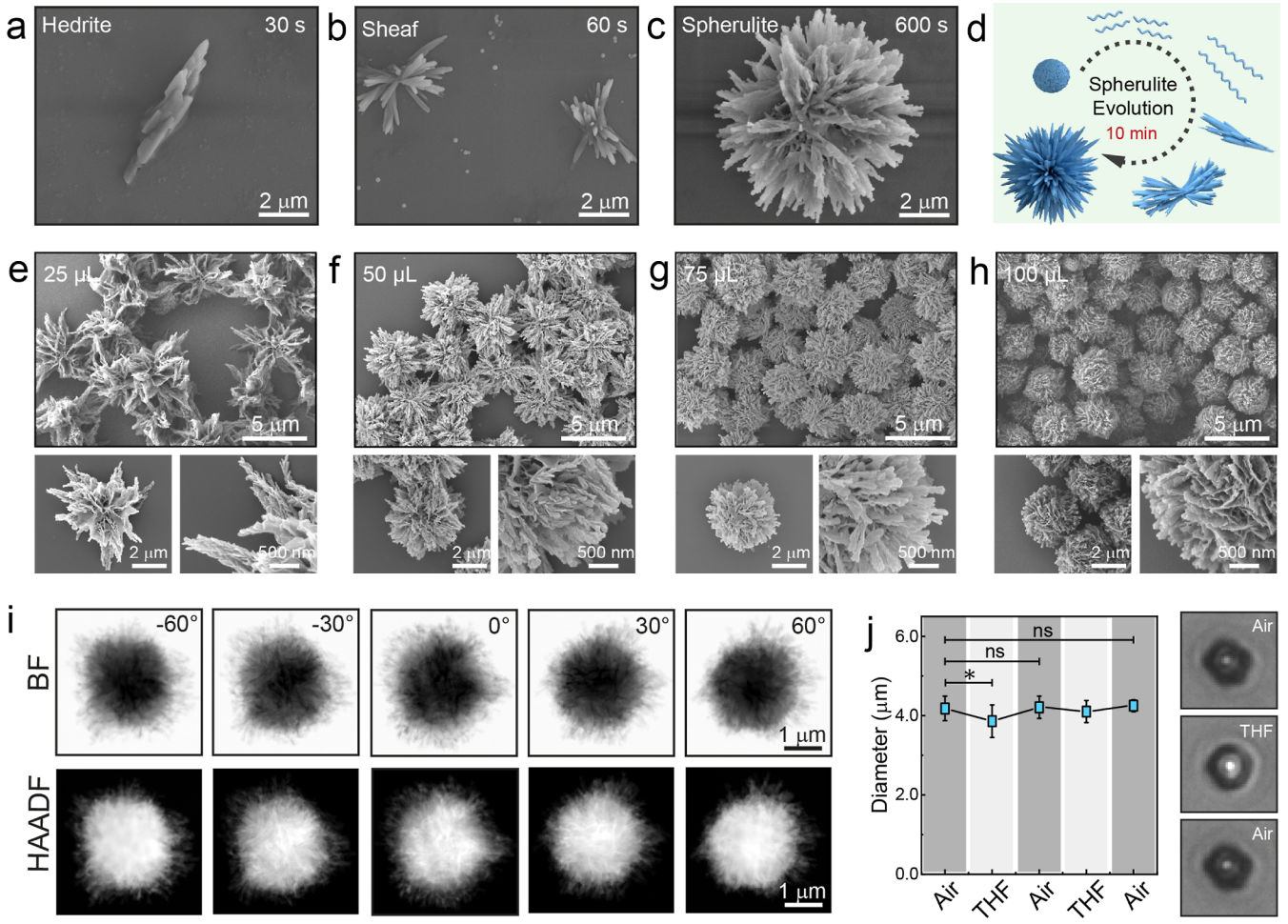

Figure 4. Spherulitic growth of rPBDT spherulites by dissolution and step-growth polymerization. (a−c) SEM images revealing the self-assembly process of PBDT into rPBDT (a: 30, b: 60, c: 600 s). (d) Schematics of rapid self-assembly process from PBDT nanoparticles. (e−h) SEM images of rPBDT spherulites prepared with different amounts of PBDT nanoparticles. (e: 25, f: 50, g: 75, h: 100 μL). (i) Bright field TEM and HAADF images of rPBDT spherulites at different tilting angles. (j) Size changes of rPBDT spherulites after soaking in THF for multiple cycles. ns means no significant difference between groups, and * means significant difference between groups.

prepared PBDT nanoparticles (15 mg mL^{-1}) of 75 μL were added into 1 mL of DMF. The initial state of the mixture dispersion was turbid due to the nanoparticle light scattering (i.e., the Tyndall effect). The material became transparent shortly due to the disassembly of nanoparticles into PBDT molecules. The sample then formed a milky dispersion again in 60 s (Figure 3a and Movie S1), thus indicating the formation of spherulites. High-angle annular dark-field (HAADF) and TEM results showed that rPBDT formed a branched spherulite with a rough surface topography and radial architecture (Figure 3b−d). Of note, the obtained spherulites were composed of S (Figure 3e), suggestive of the identical composition with PBDT nanoparticles. In the X-ray diffraction (XRD) patterns (Figure 3f), rPBDT spherulites showed peaks at 2θ = 16.5, 18.2, 19.3, 21.3, 23.4, and 26.4°, respectively, corresponding to a d-spacing of 0.53 0.49, 0.45, 0.41, 0.38, and 0.33 nm, while PBDT nanoparticles did not exhibit obvious peaks. These indicated that the dissolution and step-growth polymerization process transformed amorphous PBDT nanoparticles into crystalline rPBDT spherulites. Selected-area electron diffraction (SAED) from spikes on the rPBDT spherulites surface further confirmed the XRD structural analysis. rPBDT spherulites were crystalline with a dense core and spiky surface appearing as sharp spots in the SAED pattern (Figure 3g,h).

We further investigated the dynamic assembly of the process. Different morphologies were observed after different reaction times. rPBDT spherulites grew from hedrite to sheaf and finally became spherulite (Figures 4a−c and S4). The whole process was simple and rapid (<10 min) without complex temperature control (Figure 4d). The morphology of the spherulites was also modulated by varying the volume of the PBDT nanoparticle solution (Figures 4e−h and S5−S7). With an increase in the number of PBDT nanoparticles in the initial solution, rPBDT spherulites became smaller with denser branches. This is probably due to the generation of more spherulite nuclei at high PBDT molecules. Spherulites prepared from larger nanoparticles displayed increased dimensions and elongated aciculae, which suggests that fewer nuclei were produced when using large PBDT nanoparticles (Figure S8). This hierarchy structure endows rPBDT spherulites with a large specific surface area, which is beneficial for drug delivery application. Notably, rPBDT spherulites showed improved mechanical and colloidal properties compared to PBDT nanoparticles (Figure S9). By recording the TEM images at different tilting angles (Figure 4i), the interface between the bottom of spikelike spherulite and the underlying substrate (i.e., TEM grid) clearly showed intact boundary of the spherulites. This indicated that the PBDT nanoparticles became rigid materials after the spherulitic

https://doi.org/10.1021/jacs.3c08356
J. Am. Chem. Soc. 2023, 145, 25664−25672

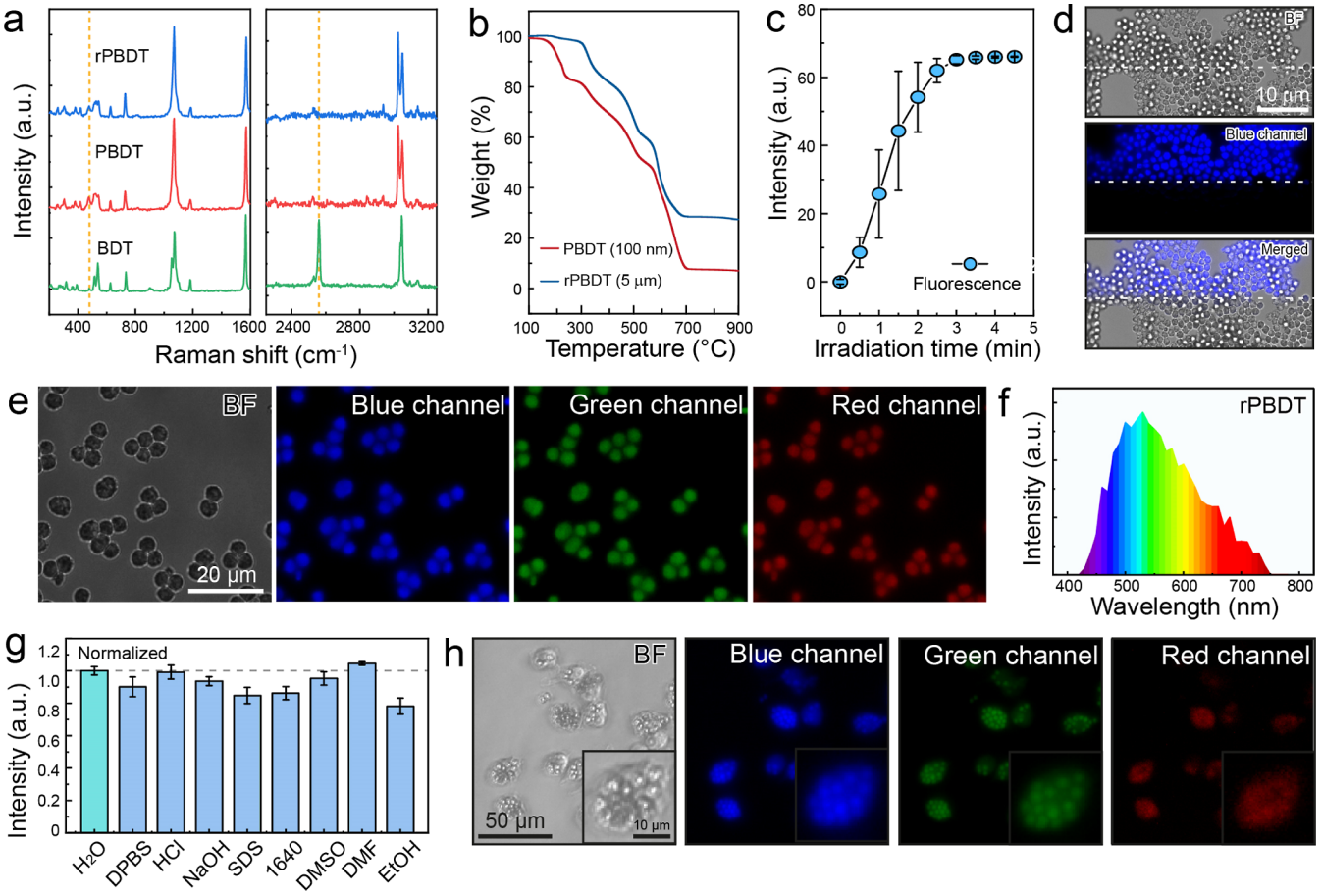

Figure 5. Molecular mechanism and luminescence properties of rPBDT spherulites. (a) Raman spectra of BDT molecules, PBDT nanoparticles, and rPBDT spherulites. (b) Thermogravimetric curves of PBDT nanoparticles and rPBDT spherulites. (c) The luminous intensity of rPBDT spherulites under different irradiation time. (d) Comparison of the luminescence characteristic of rPBDT spherulites irradiated with and without ultraviolet light. (e) Different emission of rPBDT spherulites excited in different channels (i.e., BF, blue channel, green channel, and red channel). BF: bright field; blue channel: channel with excitation wavelength of 405 nm; green channel: channel with excitation wavelength of 480 nm; red channel: channel with excitation wavelength of 560 nm. (f) The emission spectrum of rPBDT spherulites over a wide range of wavelengths (excitation at 405 nm). (g) Luminescence profile of rPBDT spherulites in different solvents (DPBS: Dulbecco's phosphate buffered saline; HCl: hydrochloric acid at pH 1; NaOH: sodium hydroxide at pH 13; sodium dodecyl sulfate buffer; 1640: RPMI-1640; DMSO; EtOH: ethanol. (h) Bright-field and fluorescent microscopy images of the raw cells after the internalization of rPBDT spherulites. Inset: higher-magnification image of a representative cell.

growth. These spherulites also exhibited excellent stability when incubated with tetrahydrofuran (THF) (Figure 4j), where the spherulites retained similar morphology during THF washing cycles, suggesting their poor solubility in THF at the current state.

The key question underneath this system is what drives the dissolved PBDT nanoparticles in DMF to form the rPBDT spherulites. Raman spectra evidenced the formation of disulfide bonds in PBDT nanoparticles and rPBDT spherulites (Figure 5a), with the disappearance of −SH (2590 cm^{-1}) and the formation of disulfide (480 cm^{-1}). Due to the poor solubility of the rPBDT spherulites in common solvent including DMF and THF, we used mass spectrometry to identify PBDT fragments after treating rPBDT with dithiothreitol (Figure S10), which also confirmed the presence of disulfide bonds. Moreover, the thermal stability of rPBDT spherulites was significantly higher than that of PBDT nanoparticles (i.e., 150 vs 300 °C) (Figures 5b and S11), which suggested a higher molecular weight of rPBDT spherulites.[52,53] We, therefore, hypothesize that the incubation of PBDT nanoparticles in DMF leads to the disruption of $\pi-\pi$ stacking and produced PBDT oligomers with active thiol terminal groups in the solution. These free thiols can form disulfide and bridge two or more oligomers into elongated rPBDT molecules, which makes rPBDT insoluble in DMF and crystallizes into spherulites. This phenomenon suggests that covalent polymerization can be employed for spherulite development, avoiding complicated assembly control (e.g., cooling and aging).

We then attempted to verify this covalent-bond-driven spherulitic formation mechanism. The formation of −S−S− depends on the oxidation of −SH by oxidant (i.e., O_2). The nitrogen atmosphere prevented the solution from becoming cloudy suggesting that the formation of spherulites is linked to the O_2 present in the system (Figure S12a,c). If the −SH groups were oxidized to $-SO_3H$ groups by H_2O_2,[54] the formation of rPBDT spherulites did not occur, indicating the pivotal role of reactive thiols in the formation of −S−S− for subsequent rPBDT spherulites (Figure S12b,c). Furthermore, we compared the disassembly behavior of rPBDT spherulites to non-cross-linked (low molecular weight) and cross-linked (high molecular weight) polystyrene (PS). The non-cross-linked PS particles, regardless of their size, were immediately dissolved in THF (Figures S13 and S14), while the morphology of the cross-linked PS particles remained basically unchanged (Figure S15). In

https://doi.org/10.1021/jacs.3c08356
J. Am. Chem. Soc. 2023, 145, 25664−25672

contrast, rPBDT spherulites remained intact in THF (Figures S16 and S17). This indicates that the high molecular weight of rPBDT spherulites resists dissolution in organic solvent.

Interestingly, rPBDT spherulites exhibited obvious luminescence (quantum yield: 4.6%) after ultraviolet light irradiation. As the irradiation pretreatment time increases, the luminescence intensity reached a maximum level (Figure 5c and Movie S2). We speculate that the luminescence properties of rPBDT spherulites are related to the formation of rigid disulfide hindering the rotation of benzene rings and the supramolecular structure of molecular chains.[55−59] The necessity for UV pretreatment can be linked to the insufficiently dense arrangement of PBDT molecules. This lack of density stems from the rapid progression of step-growth polymerization and self-assembly processes, and UV irradiation may disrupt partial disulfide bonds,[54] which leads to the reorganization of PBDT molecules within the spherulite for a more tightly packed structure. This increased structural rigidity constrains the rotation of the benzene rings within the molecular chains, allowing for the increased release of energy primarily through the fluorescence.[60] Therefore, the fluorescence intensity of rPBDT increases with prolonged irradiation time and eventually stabilizes. The optical characteristics of rPBDT spherulites without ultraviolet irradiation (Figure 5d) and PS particles (Figure S18) ruled out the potential scattering effects. Notably, these rPBDT spherulites exhibited broad emission from blue, green, to red light as they can be excited in different fluorescence channels (Figures 5e and S19). Specifically, they emitted light ranging from 430 to 750 nm (Figure 5f). We also confirmed that both PBDT nanoparticles (amorphous) and rPBDT spherulites (crystalline) exhibited similar fluorescence while the BDT molecules had no fluorescence properties (Figures S20−S23). These results collectively suggested that the crystalline degree had minor effect on the fluorescence properties. The luminescence characteristics of rPBDT spherulites are stable in diverse media even in various organic solvents (e.g., DMSO, DMF, EtOH, and THF) and harsh conditions (e.g., pH 1 or 13) (Figures 5g and S24). The LUMO and HOMO orbitals of rPBDT spherulites in different media were calculated by Gaussian simulation (Figure S25). Although the values in various solvents are different, the energy band gap is almost the same, which led to a similar luminescence performance. The broad-spectrum, stable, and uniform emission characteristics of the spherulites hold great potential for emerging white-light emission materials.[61]

We confirmed the biocompatibility of rPBDT spherulites in vitro (Figure S26). Specifically, both PBDT nanoparticles and rPBDT spherulites showed negligible cytotoxicity. This may be because of their inert and robust structure in aqueous media. Significant cellular uptake of spherulites was observed after 24 h incubation with raw cells (Figure 5h). The high cell internalization was ascribed to the spike structure of the spherulites, which facilitates the active engulfment of cells.[62,63] Moreover, the fluorescence of rPBDT was observed in the cytosol of cells. Collectively, such fluorescent spherulites exhibited great potential for traceable drug delivery due to their good biocompatibility, high porosity, superior cellular uptake, and imaging capability.

CONCLUSIONS

In summary, we report a facile synthesis of homopolymeric luminescent spherulites by a unique dissolution and reaggregation strategy. Specifically, this synthesis relies on the formation of disulfide bonds, which make shorter PBDT chains into longer rPBDT chains and then precipitate into rPBDT spherulites. The morphology of the spherulites was modulated by varying the reaction time and PBDT concentration at room temperature, avoiding complicated temperature control. The obtained spherulites exhibit excellent structural stability and tolerate various solvents. Moreover, the broad luminescence, good biocompatibility, and branched structures, combined with superior cellular uptake, make these materials attractive for intracellular drug delivery and fluorescence imaging. The simple molecule-driven spherulitic growth not only creates multifunctional hierarchical organic structures but also provides new insights for designing biomimetic architectures.

ASSOCIATED CONTENT

Supporting Information

The Supporting Information is available free of charge at https://pubs.acs.org/doi/10.1021/jacs.3c08356.

Detailed experimental procedures for PBDT nanoparticles, detailed experimental method for preparing PBDT nanoparticles by seed-mediated growth, characterization of PBDT nanoparticles, detailed preparation of rPBDT spherulites with different sizes and morphologies, and characterization of rPBDT spherulites (PDF)

MP4 (Movie S1): Changes of the solution in 60 s during the preparation of rPBDT spherulites (MP4)

MP4 (Movie S2): Increased fluorescence of rPBDT spherulites in 270 s (MP4)

AUTHOR INFORMATION

Corresponding Authors

Jiajing Zhou − *Department of Nano Engineering, University of California San Diego, La Jolla, California 92093, United States;* Present Address: College of Biomass Science and Engineering, Key Laboratory of Leather Chemistry and Engineering of Ministry of Education, National Engineering Laboratory for Clean Technology of Leather Manufacture, Sichuan University, Chengdu 610065, China; orcid.org/0000-0001-5203-4737; Email: jjzhou@scu.edu.cn

Jesse V. Jokerst − *Department of Nano Engineering, University of California San Diego, La Jolla, California 92093, United States; Materials Science and Engineering Program, University of California San Diego, La Jolla, California 92093, United States; Department of Radiology, University of California San Diego, La Jolla, California 92093, United States;* orcid.org/0000-0003-2829-6408; Email: jjokerst@ucsd.edu

Authors

Qiantao Song − *College of Biomass Science and Engineering, Key Laboratory of Leather Chemistry and Engineering of Ministry of Education, National Engineering Laboratory for Clean Technology of Leather Manufacture, Sichuan University, Chengdu 610065, China*

Yi Li − *Department of Nano Engineering, University of California San Diego, La Jolla, California 92093, United States; Department of Biomedical Engineering, McCormick School of Engineering, Northwestern University, Evanston, Illinois 60208, United States*

Zhicheng Jin − *Department of Nano Engineering, University of California San Diego, La Jolla, California 92093, United States;* orcid.org/0000-0001-6072-7533
Hai Liu − *College of Biomass Science and Engineering, Key Laboratory of Leather Chemistry and Engineering of Ministry of Education, National Engineering Laboratory for Clean Technology of Leather Manufacture, Sichuan University, Chengdu 610065, China;* orcid.org/0000-0002-4677-9617
Matthew N. Creyer − *Department of Nano Engineering, University of California San Diego, La Jolla, California 92093, United States;* orcid.org/0000-0003-1213-8245
Wonjun Yim − *Materials Science and Engineering Program, University of California San Diego, La Jolla, California 92093, United States;* orcid.org/0000-0002-0242-7898
Yanping Huang − *Center of Engineering Experimental Teaching, School of Chemical Engineering, Sichuan University, Chengdu 610065, China*
Xiaobing Hu − *The NUANCE Center, Department of Materials Science and Engineering, Northwestern University, Evanston, Illinois 60208, United States;* orcid.org/0000-0002-9233-8118
Tengyu He − *Materials Science and Engineering Program, University of California San Diego, La Jolla, California 92093, United States;* orcid.org/0000-0002-6767-4849
Yajuan Li − *Shu Chien—Gene Lay Department of Bioengineering, University of California San Diego, La Jolla, California 92093, United States*
Shana O. Kelley − *Department of Biomedical Engineering, McCormick School of Engineering, Northwestern University, Evanston, Illinois 60208, United States;* orcid.org/0000-0003-3360-5359
Lingyan Shi − *Shu Chien—Gene Lay Department of Bioengineering, University of California San Diego, La Jolla, California 92093, United States;* orcid.org/0000-0003-1373-3206

Complete contact information is available at: https://pubs.acs.org/10.1021/jacs.3c08356

Author Contributions

○Q.S. and Y.L. contributed equally.

Notes

The authors declare no competing financial interest.

■ ACKNOWLEDGMENTS

This work was performed in part at the San Diego Nanotechnology Infrastructure (SDNI) of UCSD, a member of the National Nanotechnology Coordinated Infrastructure, which is supported by the National Science Foundation (grant ECCS-2025752). We thank Dr. Bo Gao from the Analytical & Testing Center of Sichuan University for his assistance with MS characterization, Dr. Yanying Wang from Analytical & Testing Center of Sichuan University for her assistance on steady/transient fluorescence, Qingshuang Song for her assistance with DSC characterizations, and Zhonghui Wang for her assistance with confocal laser scanning microscope. Cryo-SAED patterns were collected at SKLB West China Cryo-EM Center in Sichuan University. We thank Dr. Ying Song from College of Biomass Science and Engineering at Sichuan University for her assistance in fluorescence microscopy. This work made use of the IMSERC Crystallography facility at Northwestern University, which has received support from the Soft and Hybrid Nanotechnology Experimental (SHyNE) Resource (NSF ECCS-2025633) and Northwestern University. This work made use of the EPIC facility of Northwestern University's NUANCE Center, which has received support from the SHyNE Resource (NSF ECCS-2025633), the IIN, and Northwestern's MRSEC program (NSF DMR-1720139). J.Z. acknowledges the Fundamental Research Funds for the Central Universities. M.N.C. acknowledges NIH T32 CA153915. The authors acknowledge the use of facilities and instrumentation supported by the National Science Foundation through the University of California San Diego Materials Research Science and Engineering Center DMR-2011924.

■ REFERENCES

(1) Chen, L. J.; Yang, H. B. Construction of stimuli-responsive functional materials via hierarchical self-assembly involving coordination interactions. *Acc. Chem. Res.* **2018**, *51* (11), 2699−2710.
(2) Das, K.; Gabrielli, L.; Prins, L. J. Chemically fueled self-assembly in biology and chemistry. *Angew. Chem., Int. Ed.* **2021**, *60* (37), 20120−20143.
(3) Ianiro, A.; Wu, H.; van Rijt, M. M. J.; Vena, M. P.; Keizer, A. D. A.; Esteves, A. C. C.; Tuinier, R.; Friedrich, H.; Sommerdijk, N. A. J. M.; Patterson, J. P. Liquid-liquid phase separation during amphiphilic self-assembly. *Nat. Chem.* **2019**, *11* (4), 320−328.
(4) Wang, L.; Urbas, A. M.; Li, Q. Nature-inspired emerging chiral liquid crystal nanostructures: from molecular self-assembly to DNA mesophase and nanocolloids. *Adv. Mater.* **2020**, *32* (41), 1801335.
(5) Yuan, C.; Ji, W.; Xing, R.; Li, J.; Gazit, E.; Yan, X. Hierarchically oriented organization in supramolecular peptide crystals. *Nat. Rev. Chem* **2019**, *3* (10), 567−588.
(6) Schnitzer, T.; Jansen, S. A. H.; Mabesoone, M. F. J.; Vantomme, G.; Meijer, E. W. In situ synthesis of supramolecular polymers: finding the right conditions when combining covalent and non-covalent synthesis. *Angew. Chem., Int. Ed.* **2022**, *61* (34), No. e202206729.
(7) Bai, Y.; Luo, Q.; Liu, J. Protein self-assembly via supramolecular strategies. *Chem. Soc. Rev.* **2016**, *45* (10), 2756−2767.
(8) Seeman, N. C.; Sleiman, H. F. DNA nanotechnology. *Nat. Rev. Mater.* **2017**, *3* (1), 17068.
(9) Suzuki, Y.; Endo, M.; Sugiyama, H. Lipid-bilayer-assisted two-dimensional self-assembly of DNA origami nanostructures. *Nat. Commun.* **2015**, *6*, 8052.
(10) Whitesides, G. M.; Grzybowski, B. Self-assembly at all scales. *Science* **2002**, *295* (5564), 2418−2421.
(11) Wang, H.; Feng, Z.; Xu, B. Bioinspired assembly of small molecules in cell milieu. *Chem. Soc. Rev.* **2017**, *46* (9), 2421−2436.
(12) Zhang, C.; Chen, P.; Dong, H.; Zhen, Y.; Liu, M.; Hu, W. Porphyrin supramolecular 1D structures via surfactant-assisted self-assembly. *Adv. Mater.* **2015**, *27* (36), 5379−5387.
(13) Jeong, G. H.; Sasikala, S. P.; Yun, T.; Lee, G. Y.; Lee, W. J.; Kim, S. O. Nanoscale assembly of 2D materials for energy and environmental applications. *Adv. Mater.* **2020**, *32* (35), 1907006.
(14) Ping, J.; Wang, Y.; Lu, Q.; Chen, B.; Chen, J.; Huang, Y.; Ma, Q.; Tan, C.; Yang, J.; Cao, X.; Wang, Z.; Wu, J.; Ying, Y.; Zhang, H. Self-assembly of single-layer coal-layered double hydroxide nanosheets on 3D graphene network used as highly efficient electrocatalyst for oxygen evolution reaction. *Adv. Mater.* **2016**, *28* (35), 7640−7645.
(15) Zhang, Y.; Zhang, F.; Yan, Z.; Ma, Q.; Li, X.; Huang, Y.; Rogers, J. A. Printing, folding and assembly methods for forming 3D mesostructures in advanced materials. *Nat. Rev. Mater.* **2017**, *2* (4), 17019.
(16) Yang, B.; Liu, H.; Jiang, L.; Zeng, Y.; Han, Y.; Sha, C.; Xie, X.; Li, H.; Zhou, J.; Lin, W. 3D bioprinting of collagen-based materials for oral medicine. *Collagen Leather* **2023**, *5* (1), 23.
(17) Sun, C. Y.; Marcus, M. A.; Frazier, M. J.; Giuffre, A. J.; Mass, T.; Gilbert, P. U. P. A. Spherulitic growth of coral skeletons and synthetic aragonite: nature's three-dimensional printing. *ACS Nano* **2017**, *11* (7), 6612−6622.

(18) Montanari, E.; Krupke, H.; Leroux, J. C. Engineering lipid spherulites for the sustained release of highly dosed small hydrophilic compounds. *Adv. Healthcare Mater.* **2023**, *12*, 2202249.
(19) Feng, P.; Jia, J.; Peng, S.; Shuai, Y.; Pan, H.; Bai, X.; Shuai, C. Transcrystalline growth of PLLA on carbon fiber grafted with nano-SiO_2 towards boosting interfacial bonding in bone scaffold. *Biomater. Res.* **2022**, *26* (1), 2.
(20) Li, M. C.; Wang, H. F.; Chiang, C. H.; Lee, Y. D.; Ho, R. M. Lamellar-twisting-induced circular dichroism of chromophore moieties in banded spherulites with evolution of homochirality. *Angew. Chem., Int. Ed.* **2014**, *53* (17), 4450−4455.
(21) Liu, Y.; Zhou, L.; Wen, Y.; Shen, Y.; Sun, J.; Zhou, J. Optical vector vortex generation by spherulites with cylindrical anisotropy. *Nano Lett.* **2022**, *22* (6), 2444−2449.
(22) Macias-Sanchez, E.; Tarakina, N. V.; Ivanov, D.; Blouin, S.; Berzlanovich, A. M.; Fratzl, P. Spherulitic crystal growth drives mineral deposition patterns in collagen-based materials. *Adv. Funct.* **2022**, *32* (31), 1603514.
(23) Shtukenberg, A. G.; Punin, Y. O.; Gunn, E.; Kahr, B. Spherulites. *Chem. Rev.* **2012**, *112* (3), 1805−1838.
(24) Exley, C.; House, E.; Collingwood, J. F.; Davidson, M. R.; Cannon, D.; Donald, A. M. Spherulites of amyloid-β_{42} in vitro and in Alzheimer's disease. *J. Alzheimer's Dis.* **2010**, *20* (4), 1159−1165.
(25) Sigurdson, C. J.; Joshi-Barr, S.; Bett, C.; Winson, O.; Manco, G.; Schwarz, P.; Rülicke, T.; Nilsson, K. P. R.; Margalith, I.; Raeber, A.; Peretz, D.; Hornemann, S.; Wüthrich, K.; Aguzzi, A. Spongiform encephalopathy in transgenic mice expressing a point mutation in the β2-α2 loop of the prion protein. *J. Neurosci.* **2011**, *31* (39), 13840−13847.
(26) Krebs, M. R. H.; MacPhee, C. E.; Miller, A. F.; Dunlop, I. E.; Dobson, C. M.; Donald, A. M. The formation of spherulites by amyloid fibrils of bovine insulin. *Proc. Natl. Acad. Sci. U.S.A.* **2004**, *101* (40), 14420−14424.
(27) Krebs, M. R. H.; Bromley, E. H. C.; Donald, A. M. The binding of thioflavin-T to amyloid fibrils: localisation and implications. *J. Struct. Biol.* **2005**, *149* (1), 30−37.
(28) Vetri, V.; Piccirilli, F.; Krausser, J.; Buscarino, G.; Lapinska, U.; Vestergaard, B.; Zaccone, A.; Fodera, V. Ethanol controls the self-assembly and mesoscopic properties of human insulin amyloid spherulites. *J. Phys. Chem. B* **2018**, *122* (12), 3101−3112.
(29) Shtukenberg, A. G.; Freudenthal, J.; Kahr, B. Reversible twisting during helical hippuric acid crystal growth. *J. Am. Chem. Soc.* **2010**, *132* (27), 9341−9349.
(30) Kennedy, M.; Turturro, G.; Brown, G. R.; Stpierre, L. E. Silica retards radial growth of spherulites in isotactic polystyrene. *Nature* **1980**, *287* (5780), 316−317.
(31) Xing, P. X.; Dong, L. S.; An, Y. X.; Feng, Z. L.; Avella, M.; Martuscelli, E. Miscibility and crystallization of poly(β-hydroxybutyrate) and poly(p-vinylphenol) blends. *Macromolecules* **1997**, *30* (9), 2726−2733.
(32) Crist, B.; Schultz, J. M. Polymer spherulites: a critical review. *Prog. Polym. Sci.* **2016**, *56*, 1−63.
(33) Magill, J. H. Review spherulites: a personal perspective. *J. Mater. Sci.* **2001**, *36* (13), 3143−3164.
(34) Bobrov, G.; Kedzior, S. A.; Pervez, S. A.; Govedarica, A.; Kloker, G.; Fichtner, M.; Michaelis, V. K.; Bernard, G. M.; Veelken, P. M.; Hausen, F.; Trifkovic, M. Coupling particle ordering and spherulitic growth for long-term performance of nanocellulose/poly(ethylene oxide) electrolytes. *ACS Appl. Mater.* **2023**, *15* (1), 1996−2008.
(35) Gautier, L.; Cazottes, S.; Veron, M.; Fabregue, D.; Chevalier, J. Spherulitic growth process in Ti-based metallic glass: microstructure, phase identification, and growth mechanism. *Mater. Charact.* **2022**, *192*, 112170.
(36) Kwak, H.; Kim, H.; Park, S. A.; Lee, M.; Jang, M.; Park, S. B.; Hwang, S. Y.; Kim, H. J.; Jeon, H.; Koo, J. M.; Park, J.; Oh, D. X. Biodegradable, water-resistant, anti-fizzing, polyester nanocellulose composite paper straws. *Adv. Sci.* **2023**, *10* (1), 2205554.
(37) Liu, Y.; Guan, Y.; Zhai, J.; Zhang, L.; Lin, J.; Chen, F. Study on in situ visualization crystallization behavior and secondary nucleation model of polypropylene under supercritical N_2. *Compos. Sci. Technol.* **2022**, *230* (1), 109770.
(38) Zhu, Q.; Shtukenberg, A. G.; Carter, D. J.; Yu, T. Q.; Yang, J. X.; Chen, M.; Raiteri, P.; Oganov, A. R.; Pokroy, B.; Polishchuk, I.; Bygrave, P. J.; Day, G. M.; Rohl, A. L.; Tuckerman, M. E.; Kahr, B. Resorcinol crystallization from the melt: a new ambient phase and new "riddles". *J. Am. Chem. Soc.* **2016**, *138* (14), 4881−4889.
(39) Lugito, G.; Woo, E. M.; Hsieh, Y. T. Transitional ring bands constructed by discrete positive- and negative-birefringence lamellae packed in poly(1,6-hexamethylene adipate) spherulites. *Macromolecules* **2015**, *48* (21), 7953−7967.
(40) Sasaki, T.; Asakawa, R.; Sakurai, K. Formation of porous spherulites of poly(L-lactide) grown from solutions. *Polym. J.* **2009**, *41* (9), 787−791.
(41) Li, Y.; Wang, Z.; He, T. Morphological control of polymer spherulites via manipulating radial lamellar organization upon evaporative crystallization: a mini review. *Crystals* **2017**, *7* (4), 115.
(42) Lotz, B.; Cheng, S. Z. D. A critical assessment of unbalanced surface stresses as the mechanical origin of twisting and scrolling of polymer crystals. *Polymer* **2005**, *46* (3), 577−610.
(43) Jiang, J.; Nikbin, E.; Hicks, G.; Song, S.; Liu, Y.; Wong, E. C. N.; Manners, I.; Howe, J. Y.; Winnik, M. A. Polyferrocenylsilane block copolymer spherulites in dilute solution. *J. Am. Chem. Soc.* **2023**, *145*, 1247−1261.
(44) Song, S. F.; Zhou, H.; Ye, S. Y.; Tam, J.; Howe, J. Y.; Manners, I.; Winnik, M. A. Spherulite-like micelles. *Angew. Chem., Int. Ed.* **2021**, *60* (19), 10950−10956.
(45) Wen, T.; Wang, H. F.; Li, M. C.; Ho, R. M. Homochiral evolution in self-assembled chiral polymers and block copolymers. *Acc. Chem. Res.* **2017**, *50* (4), 1011−1021.
(46) Shtukenberg, A. G.; Punin, Y. O.; Gujral, A.; Kahr, B. Growth actuated bending and twisting of single crystals. *Angew. Chem., Int. Ed.* **2014**, *53* (3), 672−699.
(47) Zhou, J.; Xu, M.; Jin, Z.; Borum, R. M.; Avakyan, N.; Cheng, Y.; Yim, W.; He, T.; Zhou, J.; Wu, Z.; Mantri, Y.; Jokerst, J. V. Versatile polymer nanocapsules via redox competition. *Angew. Chem., Int. Ed.* **2021**, *60* (50), 26357−26362.
(48) Zhou, J.; Creyer, M. N.; Chen, A.; Yim, W.; Lafleur, R. P. M.; He, T.; Lin, Z.; Xu, M.; Abbasi, P.; Wu, J.; Pascal, T. A.; Caruso, F.; Jokerst, J. V. Stereoselective growth of small molecule patches on nanoparticles. *J. Am. Chem. Soc.* **2021**, *143* (31), 12138−12144.
(49) Zhao, P.; Li, N.; Astruc, D. State of the art in gold nanoparticle synthesis. *Coord. Chem. Rev.* **2013**, *257* (3−4), 638−665.
(50) Qiu, H.; Gao, Y.; Boott, C. E.; Gould, O. E. C.; Harniman, R. L.; Miles, M. J.; Webb, S. E. D.; Winnik, M. A.; Manners, I. Uniform patchy and hollow rectangular platelet micelles from crystallizable polymer blends. *Science* **2016**, *352* (6286), 697−701.
(51) Zhou, J.; Lin, Z.; Penna, M.; Pan, S.; Ju, Y.; Li, S.; Han, Y.; Chen, J.; Lin, G.; Richardson, J. J.; Yarovsky, I.; Caruso, F. Particle engineering enabled by polyphenol-mediated supramolecular networks. *Nat. Commun.* **2020**, *11* (1), 4804.
(52) Xie, R.; Weisen, A. R.; Lee, Y.; Aplan, M. A.; Fenton, A. M.; Masucci, A. E.; Kempe, F.; Sommer, M.; Pester, C. W.; Colby, R. H.; Gomez, E. D. Glass transition temperature from the chemical structure of conjugated polymers. *Nat. Commun.* **2020**, *11* (1), 893.
(53) Kochi, T.; Noda, S.; Yoshimura, K.; Nozaki, K. Formation of linear copolymers of ethylene and acrylonitrile catalyzed by phosphine sulfonate palladium complexes. *J. Am. Chem. Soc.* **2007**, *129* (29), 8948−8949.
(54) Jin, Z.; Sugiyama, Y.; Zhang, C.; Palui, G.; Xin, Y.; Du, L.; Wang, S.; Dridi, N.; Mattoussi, H. Rapid photoligation of gold nanocolloids with lipoic acid-based ligands. *Chem. Mater.* **2020**, *32* (17), 7469−7483.
(55) Liu, B.; Zhang, H. K.; Liu, S. J.; Sun, J. Z.; Zhang, X. H.; Tang, B. Z. Polymerization-induced emission. *Mater. Horizons.* **2020**, *7* (4), 987−998.
(56) Li, J.; Pu, K. Development of organic semiconducting materials for deep-tissue optical imaging, phototherapy and photoactivation. *Chem. Soc. Rev.* **2019**, *48* (1), 38−71.

https://doi.org/10.1021/jacs.3c08356
J. Am. Chem. Soc. 2023, 145, 25664−25672

(57) Liao, P. L.; Huang, J. B.; Yan, Y.; Tang, B. Z. Clusterization-triggered emission (CTE): one for all, all for one. *Mater. Chem. Front.* **2021**, *5* (18), 6693−6717.
(58) Fowler, W. C. Intrinsic fluorescence in peptide amphiphile micelles with protein-inspired phosphate sensing. *Biomacromolecules* **2022**, *23* (11), 4804−4813.
(59) Yu, Y.; Gim, S.; Kim, D.; Arnon, Z. A.; Gazit, E.; Seeberger, P. H.; Delbianco, M. Oligosaccharides self-assemble and show intrinsic optical properties. *J. Am. Chem. Soc.* **2019**, *141* (12), 4833−4838.
(60) Zhang, J.; He, B.; Hu, Y.; Alam, P.; Zhang, H.; Lam, J. W. Y.; Tang, B. Z. Stimuli-responsive AIEgens. *Adv. Mater.* **2021**, *33* (32), 2008071.
(61) Wang, J. G.; Gu, X. G.; Ma, H. L.; Peng, Q.; Huang, X. B.; Zheng, X. Y.; Sung, S. H. P.; Shan, G. G.; Lam, J. W. Y.; Shuai, Z. G.; Tang, B. Z. A facile strategy for realizing room temperature phosphorescence and single molecule white light emission. *Nat. Commun.* **2018**, *9* (1), 2963.
(62) Huang, L. L.; Mao, X. H.; Li, J.; Li, Q.; Shen, J. L.; Liu, M. M.; Fan, C. H.; Tian, Y. Nanoparticle spikes enhance cellular uptake via regulating myosin IIA recruitment. *ACS Nano* **2023**, *17* (10), 9155−9166.
(63) Chen, H. J.; Hang, T.; Yang, C.; Liu, D.; Su, C.; Xiao, S.; Liu, C.; Lin, D.-a.; Zhang, T.; Jin, Q.; Tao, J.; Wu, M. X.; Wang, J.; Xie, X. Functionalized spiky particles for intracellular biomolecular delivery. *ACS Cent. Sci.* **2019**, *5* (6), 960−969.

https://doi.org/10.1021/jacs.3c08356
J. Am. Chem. Soc. 2023, 145, 25664−25672